Electronic Supplementary Information (ESI)

8-Hydroxyquinolinate-Based Metal–Organic Frameworks: Synthesis, Tunable Luminescent Properties, and Highly Sensitive Detection of Small Molecules and Metal Ions

Xiangxiang Zhao, Shilin Wang, Liyan Zhang, Suya Liu, and Guozan Yuan*

School of Chemistry and Chemical Engineering, Anhui University of Technology, Maanshan, 243032, P. R. China；

Corresponding Author E-mail: yuanguozan@163.com

Table of Contents

Table S1. Crystal data and structure refinement for **1**-**3.**
Table S2. Table S2 Crystal data and structure refinement for **4** and **5.**
Table S3-7 Selected bond lengths [Å] and angles [º] for **1-5**.
Figure S1. ^{1}H and ^{13}C NMR spectroscopy of H_2L.
Figure S2. ESI-MS spectrum of H_2L.
Figure S3. FTIR spectra of complexes **1-5**.
Figure S4-21. Views of the crystal structures of complexes **1-5**.
Figure S22. PXRD patterns of complexes **1-5**.
Figure S23. TGA plots for complexes **1-5**.
Figure S24. Fluorescence decay curves of complexes **1**-**3** in the solid state.
Figure S25. The fluorescence intensities of **1** in various organic molecules.
Figure S26. Fluorescence spectra of **1** upon addition of various amounts of nitroaromatics.
Figure S27. Luminescence spectra and intensity of **1** treated with various aromatic analytes.
Figure S28. Upon addition of different Ln^{3+} cations, luminescence behavior of suspension of **1**.
Figure S29. Luminescence intensities of **1** immersed in the individual aqueous solutions of $Ln(NO_3)_3$ and mixed metal ions including Fe^{3+} ion under an excitation of 350 nm.
Figure S30. The reversibility test for sensing Fe^{3+}. Emission intensity of **1**, Fe@**1**, @**1**, 2nd, 5th.
Figure S31. PXRD patterns of **1** dispersed in water, iron(III) nitrate solution and the recycled sample.
Figure S32. Variation of fluorescence intensities of complex **1** immersed in the aqueous solutions with different concentrations of $Fe(NO_3)_3$.
Figure S33. The fitting plot of the quenching efficiency with the increasing concentration of Fe^{3+} in the low concentration range.
Figure S34. The UV−vis absorption spectra of aqueous solutions containing various mental ions.
Figure S35. The UV−vis absorption spectra of Fe^{3+} with a gradual increase in concentration.

Table S1. Crystal data and structure refinement for **1**-**3**.

Complex	**1**	**2**	**3**
Formula	$C_{22}H_{22}N_2O_5Zn$	$C_{46}H_{32}N_4O_6Zn_2$	$C_{36}H_{28}N_2O_9Cd_2$
F_w	458.08	867.49	857.40
cryst syst	monoclinic	triclinic	Orthorhombic
space group	$P2_1/n$	$P\bar{1}$	$Pbca$
a (Å)	14.007(6)	9.155(1)	20.7834(3)
b (Å)	9.850(4)	11.355(2)	9.9638(2)
c (Å)	16.808(7)	19.659(3)	39.8759(6)
α (deg)	90	97.96(2)	90
β (deg)	111.33(5)	100.35(2)	90
γ (deg)	90	100.55(2)	90
V (Å^3)	2160.1(2)	1945.0(5)	8257.6(2)
Z	4	2	8
D_c (g.cm^{-3})	1.401	1.481	1.379
F(000)	936	888	3408
μ (mm^{-1})	1.171	1.290	5.885
T (K)	296	296	170.0
reflns/unique	10814/3796	10039/6731	58823/7076
R_{int}	0.0537	0.0195	0.0588
data/restraints/params	3796/244/262	6731/0/523	7076/6/442
GOF on F^2	1.045	1.055	1.050
R_1, wR_2 ($I > 2\sigma(I)$)	0.0579, 0.1572	0.0362, 0.0978	0.0602, 0.1640
R_1, wR_2 (all data)	0.0891, 0.1852	0.0481, 0.1047	0.0715, 0.1728
largest diff. peak and hole (e.Å^{-3})	1.218, -0.435	0.446, -0.347	2.72, -1.37

Table S2. Crystal data and structure refinement for **4** and **5**.

Complex	**4**	**5**
Formula	$C_{22}H_{22}N_2O_5Mn$	$C_{21}H_{22}N_2O_6Co$
F_w	445.32	457.08
cryst syst	monoclinic	monoclinic
space group	$P2_1/n$	$P2_1/n$
a (Å)	14.237(9)	14.2987(3)
b (Å)	9.826(6)	9.5698(2)
c (Å)	16.813(11)	16.5088(3)
α (deg)	90	90
β (deg)	111.30(7)	111.3900(10)
γ (deg)	90	90
V (Å^3)	2191(2)	2103.39(7)
Z	4	4
D_c (g.cm^{-3})	1.350	1.431
F(000)	916	932
μ (mm^{-1})	0.636	0.855
T (K)	296	170(2)
reflns/unique	10917/3845	12284/3947
R_{int}	0.0277	0.0568
data/restraints/params	3845/0/262	3947/0/270
GOF on F^2	1.068	1.070
R_1, wR_2 ($I > 2\sigma(I)$)	0.0469, 0.1432	0.0585, 0.1614
R_1, wR_2 (all data)	0.0594, 0.1572	0.0638, 0.1651
largest diff. peak and hole (e.Å^{-3})	0.613, -0.306	0.749, -0.742

Table S3. Selected bond lengths [Å] and angles [º] for **1**.

Zn(1)-O(2)#1	1.973(4)	O(2)#1-Zn(1)-N(1)	95.97(16)
Zn(1)-O(4)	2.035(4)	O(4)-Zn(1)-N(1)	97.96(14)
Zn(1)-O(1)	2.042(3)	O(1)-Zn(1)-N(1)	77.19(14)
Zn(1)-O(1)#2	2.065(3)	O(1)#2-Zn(1)-N(1)	152.19(14)
Zn(1)-N(1)	2.195(4)	C(1)-O(1)-Zn(1)	114.9(3)
O(2)#1-Zn(1)-O(4)	100.25(16)	C(1)-O(1)-Zn(1)#2	136.8(3)
O(2)#1-Zn(1)-O(1)	145.35(17)	Zn(1)-O(1)-Zn(1)#2	104.96(15)
O(4)-Zn(1)-O(1)	114.28(15)	C(9)-N(1)-Zn(1)	129.4(3)
O(2)#1-Zn(1)-O(1)#2	105.96(16)	C(6)-N(1)-Zn(1)	110.3(3)
O(4)-Zn(1)-O(1)#2	94.80(15)	C(18)-O(2)-Zn(1)#4	107.5(4)
O(1)-Zn(1)-O(1)#2	75.04(15)	C(19)-O(4)-Zn(1)	117.9(3)

Symmetry transformations used to generate equivalent atoms:

#1 -x+1/2, y-1/2, -z+1/2 #2 -x, -y+1, -z+1

#3 -x+1, -y+1, -z+1 #4 -x+1/2, y+1/2, -z+1/2

Table S4. Selected bond lengths [Å] and angles [º] for **2**.

Zn(1)-O(5)#1	1.972(2)	C(6)-N(1)-Zn(1)	108.76(17)
Zn(1)-O(1)	1.9970(19)	O(4)-Zn(2)-O(2)	145.80(9)
Zn(1)-N(2)	2.093(2)	O(4)-Zn(2)-N(4)	98.41(10)
Zn(1)-O(1)#2	2.1165(19)	O(2)-Zn(2)-N(4)	114.54(9)
Zn(1)-N(1)	2.224(2)	O(4)-Zn(2)-O(2)#3	96.99(8)
Zn(2)-O(4)	1.957(2)	O(2)-Zn(2)-O(2)#3	74.39(9)
Zn(2)-O(2)	1.9901(18)	N(4)-Zn(2)-O(2)#3	91.22(9)
Zn(2)-N(4)	2.086(2)	O(4)-Zn(2)-N(3)	106.85(9)
Zn(2)-O(2)#3	2.155(2)	O(2)-Zn(2)-N(3)	78.73(8)
Zn(2)-N(3)	2.197(2)	N(4)-Zn(2)-N(3)	97.53(9)
O(5)#1-Zn(1)-O(1)	152.40(10)	O(2)#3-Zn(2)-N(3)	152.99(8)
O(5)#1-Zn(1)-N(2)	99.06(10)	C(19)-O(2)-Zn(2)	117.20(17)
O(1)-Zn(1)-N(2)	108.38(10)	C(19)-O(2)-Zn(2)#3	136.10(17)
O(5)#1-Zn(1)-O(1)#2	97.68(8)	Zn(2)-O(2)-Zn(2)#3	105.61(9)
O(1)-Zn(1)-O(1)#2	75.14(8)	C(41)-N(2)-Zn(1)	121.7(2)
N(2)-Zn(1)-O(1)#2	100.03(9)	C(37)-N(2)-Zn(1)	120.0(2)
O(5)#1-Zn(1)-N(1)	106.24(9)	C(27)-N(3)-Zn(2)	131.37(19)
O(1)-Zn(1)-N(1)	78.45(8)	C(24)-N(3)-Zn(2)	108.86(17)
N(2)-Zn(1)-N(1)	87.32(9)	C(18)-O(4)-Zn(2)	117.9(2)
O(1)#2-Zn(1)-N(1)	153.57(8)	C(46)-N(4)-Zn(2)	121.8(2)
C(1)-O(1)-Zn(1)	117.43(17)	C(42)-N(4)-Zn(2)	120.8(2)
C(1)-O(1)-Zn(1)#2	137.57(17)	C(36)-O(5)-Zn(1)#4	107.3(2)
C(9)-N(1)-Zn(1)	131.56(19)		

Symmetry transformations used to generate equivalent atoms:

#1 x+1, y, z #2 -x+2, -y+2, -z+1 #3 -x, -y, -z

#4 x-1, y, z

Table S5. Selected bond lengths [Å] and angles [º] for **3**.

Cd(1)-O(9)	2.380(5)	O(3)-Cd(1)-O(4)	175.39(16)
Cd(1)-O(4)#1	2.286(4)	O(3)-Cd(1)-O(4)#1	103.49(16)
Cd(1)-O(4)	2.258(4)	O(3)-Cd(1)-N(1)	112.20(17)
Cd(1)-O(3)	2.232(5)	O(3)-Cd(1)-N(2)	71.76(19)
Cd(1)-N(1)	2.370(4)	N(1)-Cd(1)-O(9)	88.54(18)
Cd(1)-N(2)	2.447(5)	N(1)-Cd(1)-N(2)	98.12(15)
Cd(2)-O(6)	2.366(6)	O(6)-Cd(2)-O(1)#2	92.9(2)
Cd(2)-O(1)#2	2.371(6)	O(6)-Cd(2)-O(5)	53.1(3)
Cd(2)-O(5)	2.486(7)	O(6)-Cd(2)-O(2)#2	145.3(2)
Cd(2)-O(7)	2.289(9)	O(1)#2-Cd(2)-O(5)	92.3(3)
Cd(2)-O(2)#2	2.398(6)	O(1)#2-Cd(2)-O(2)#2	54.4(2)
Cd(2)-O(8)	2.223(8)	O(7)-Cd(2)-O(6)	85.0(3)
O(9)-Cd(1)-N(2)	155.5(2)	O(7)-Cd(2)-O(1)#2	95.8(3)
O(4)#1-Cd(1)-O(9)	90.56(18)	O(7)-Cd(2)-O(5)	137.7(3)
O(4)-Cd(1)-O(9)	96.3(2)	O(7)-Cd(2)-O(2)#2	107.5(3)
O(4)-Cd(1)-O(4)#1	71.90(16)	O(2)#2-Cd(2)-O(5)	110.9(3)
O(4)-Cd(1)-N(1)	72.41(14)	O(8)-Cd(2)-O(6)	123.0(3)
O(4)#1-Cd(1)-N(1)	143.97(15)	O(8)-Cd(2)-O(1)#2	136.3(3)
O(4)#1-Cd(1)-N(2)	97.45(15)	O(8)-Cd(2)-O(5)	91.2(3)
O(4)-Cd(1)-N(2)	108.19(16)	O(8)-Cd(2)-O(7)	110.2(3)
O(3)-Cd(1)-O(9)	83.8(2)	O(8)-Cd(2)-O(2)#2	83.8(3)

Symmetry transformations used to generate equivalent atoms:
#1 1-X, 1-Y, 1-Z; #2 +X, 1/2-Y, -1/2+Z

Table S6. Selected bond lengths [Å] and angles [º] for **4**.

Mn(1)-O(3)#1	2.106(3)	O(4)-Mn(1)-O(2)#1	153.48(9)
Mn(1)-O(1)#2	2.128(2)	N(1)-Mn(1)-O(2)#1	88.53(9)
Mn(1)-O(1)	2.137(2)	O(3)#1-Mn(1)-C(18)#1	28.94(11)
Mn(1)-O(4)	2.141(3)	O(1)#2-Mn(1)-C(18)#1	107.34(10)
Mn(1)-N(1)	2.309(2)	O(1)-Mn(1)-C(18)#1	123.75(12)
Mn(1)-O(2)#1	2.483(3)	O(4)-Mn(1)-C(18)#1	125.90(12)
Mn(1)-C(18)#1	2.610(4)	N(1)-Mn(1)-C(18)#1	90.98(10)
O(3)#1-Mn(1)-O(1)#2	111.13(10)	O(2)#1-Mn(1)-C(18)#1	27.72(10)
O(3)#1-Mn(1)-O(1)	152.33(11)	C(1)-O(1)-Mn(1)#2	136.03(18)
O(1)#2-Mn(1)-O(1)	75.99(9)	C(1)-O(1)-Mn(1)	117.69(18)
O(3)#1-Mn(1)-O(4)	96.98(10)	Mn(1)#2-O(1)-Mn(1)	104.01(9)
O(1)#2-Mn(1)-O(4)	91.74(9)	C(9)-N(1)-Mn(1)	128.36(19)
O(1)-Mn(1)-O(4)	109.75(9)	C(6)-N(1)-Mn(1)	110.78(17)
O(3)#1-Mn(1)-N(1)	96.77(11)	C(18)-O(2)-Mn(1)#4	81.9(2)
O(1)#2-Mn(1)-N(1)	149.51(8)	C(18)-O(3)-Mn(1)#4	98.0(2)
O(1)-Mn(1)-N(1)	73.56(9)	C(19)-O(4)-Mn(1)	119.8(2)

O(4)-Mn(1)-N(1)	97.00(9)	O(2)-C(18)-Mn(1)#4	70.4(2)
O(3)#1-Mn(1)-O(2)#1	56.54(10)	O(3)-C(18)-Mn(1)#4	53.04(17)
O(1)#2-Mn(1)-O(2)#1	96.55(9)	C(15)-C(18)-Mn(1)#4	166.3(3)
O(1)-Mn(1)-O(2)#1	96.71(9)		

Symmetry transformations used to generate equivalent atoms:

#1 -x+3/2, y+1/2, -z+3/2 #2 -x+1, -y, -z+2

#3 -x+1, -y+1, -z+1 #4 -x+3/2, y-1/2, -z+3/2

Table S7. Selected bond lengths [Å] and angles [º] for **5**.

N(1)-Co(1)	2.162(3)	C(19)-O(4)-Co(1)	118.4(2)
O(1)-Co(1)	2.022(2)	O(1)-Co(1)-O(4)	108.73(10)
O(1)-Co(1)#2	2.093(2)	O(1)-Co(1)-O(3)#3	157.60(11)
O(2)-Co(1)#1	2.352(3)	O(4)-Co(1)-O(3)#3	93.67(11)
O(3)-Co(1)#1	2.056(3)	O(1)-Co(1)-O(1)#2	75.95(10)
O(4)-Co(1)	2.056(2)	O(4)-Co(1)-O(1)#2	92.52(10)
Co(1)-O(3)#3	2.056(3)	O(3)#3-Co(1)-O(1)#2	103.48(11)
Co(1)-O(1)#2	2.094(2)	O(1)-Co(1)-N(1)	78.52(10)
Co(1)-O(2)#3	2.352(3)	O(4)-Co(1)-N(1)	97.03(10)
C(9)-N(1)-Co(1)	130.9(2)	O(3)#3-Co(1)-N(1)	99.52(11)
C(6)-N(1)-Co(1)	109.2(2)	O(1)#2-Co(1)-N(1)	154.43(9)
C(1)-O(1)-Co(1)	114.9(2)	O(1)-Co(1)-O(2)#3	98.70(9)
C(1)-O(1)-Co(1)#2	137.2(2)	O(4)-Co(1)-O(2)#3	152.53(9)
Co(1)-O(1)-Co(1)#2	104.05(10)	O(3)#3-Co(1)-O(2)#3	58.91(10)
C(18)-O(2)-Co(1)#1	82.6(2)	O(1)#2-Co(1)-O(2)#3	95.50(10)
C(18)-O(3)-Co(1)#1	95.8(2)	N(1)-Co(1)-O(2)#3	86.86(10)

Symmetry transformations used to generate equivalent atoms:

#1 -x+1/2, y+1/2, -z+3/2 #2 -x+1, -y+1, -z+1

#3 -x+1/2, y-1/2, -z+3/2

Figure S1. (a) ^{1}H and (b) ^{13}C NMR spectra of H_2L.

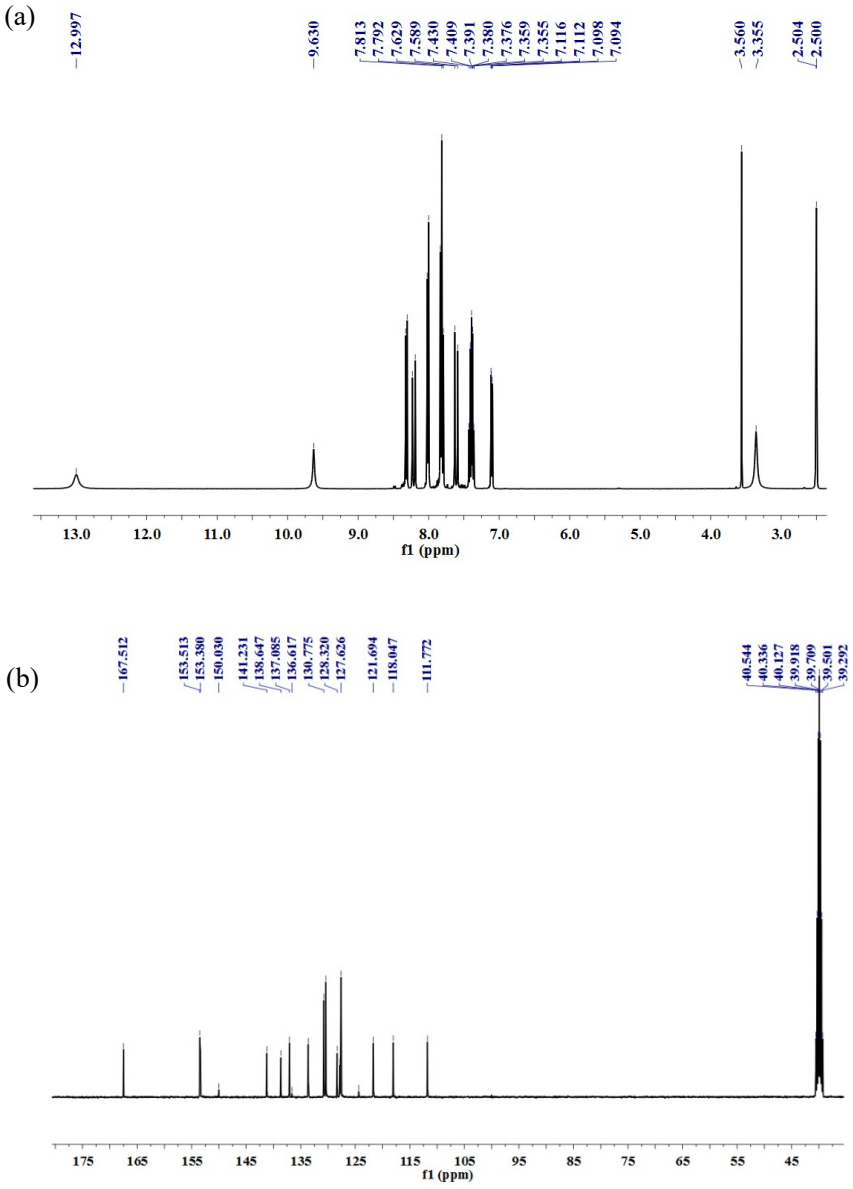

Figure S2. ESI-MS spectroscopy of H_2L.

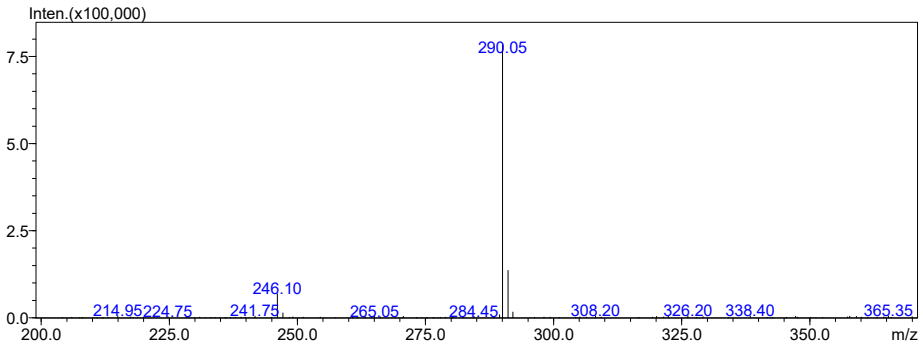

Figure S3. FTIR spectra of complexes **1**-**5**.

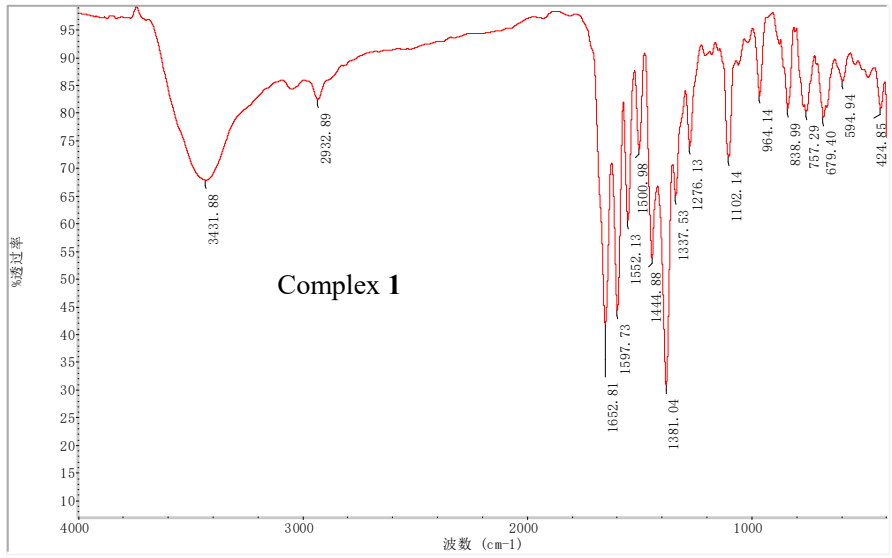

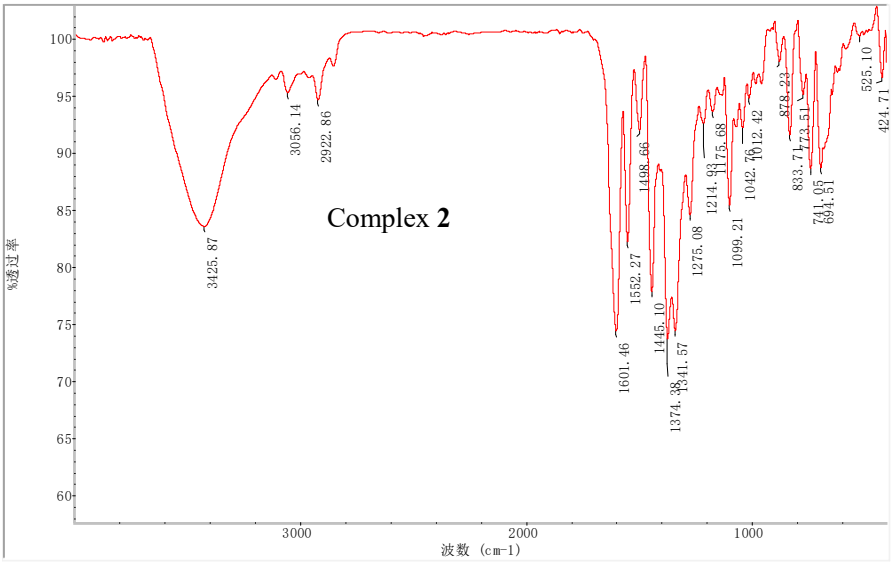

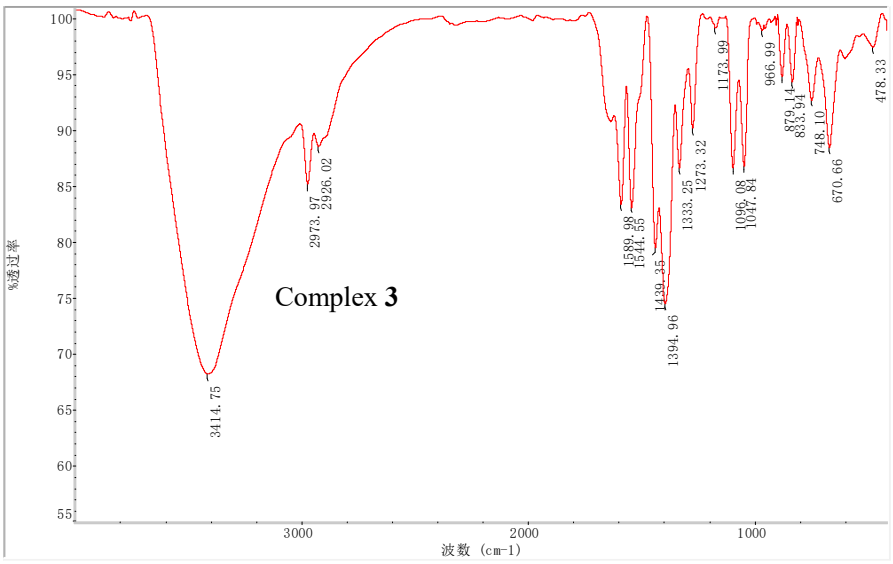

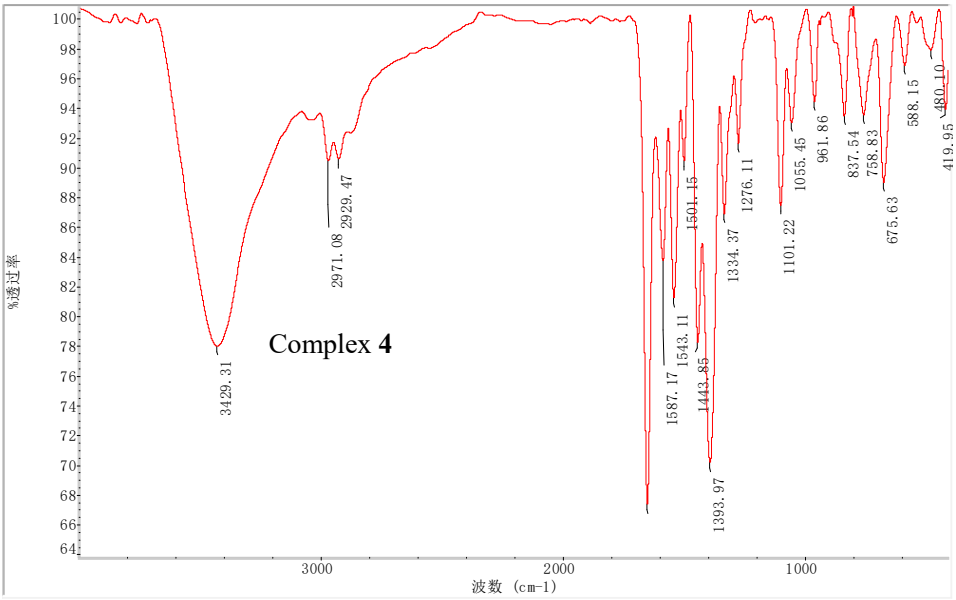
Complex 4
%透过率
波数 (cm-1)
3429.31
2971.08
2929.47
1587.17
1543.11
1501.15
1443.85
1393.97
1334.37
1276.11
1101.22
1055.45
961.86
837.54
758.83
675.63
588.15
480.10
419.95

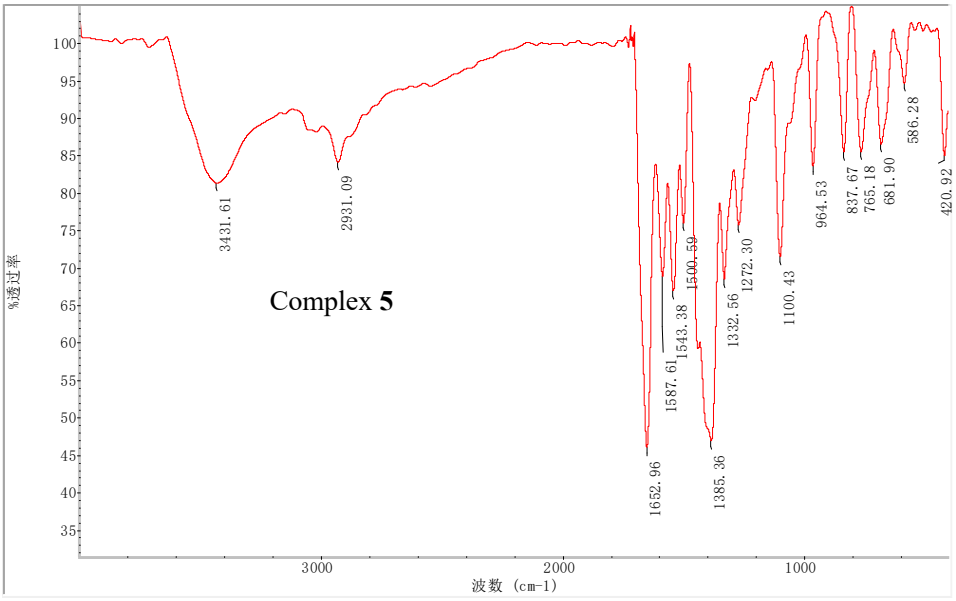
Complex 5
%透过率
波数 (cm-1)
3431.61
2931.09
1652.96
1587.61
1543.38
1500.59
1385.36
1332.56
1272.30
1100.43
964.53
837.67
765.18
681.90
586.28
420.92

Figure S4. View of the asymmetric unit of **1.**

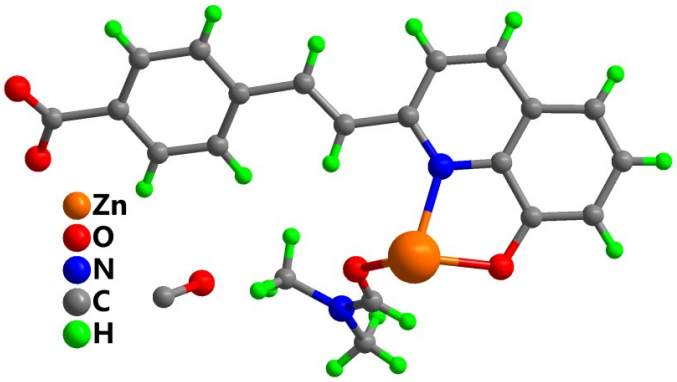

Figure S5. Perspective view of C–H···O and C–H···N intermolecular interactions in **1** (Zn: green; O: red; N: blue; C: gray).

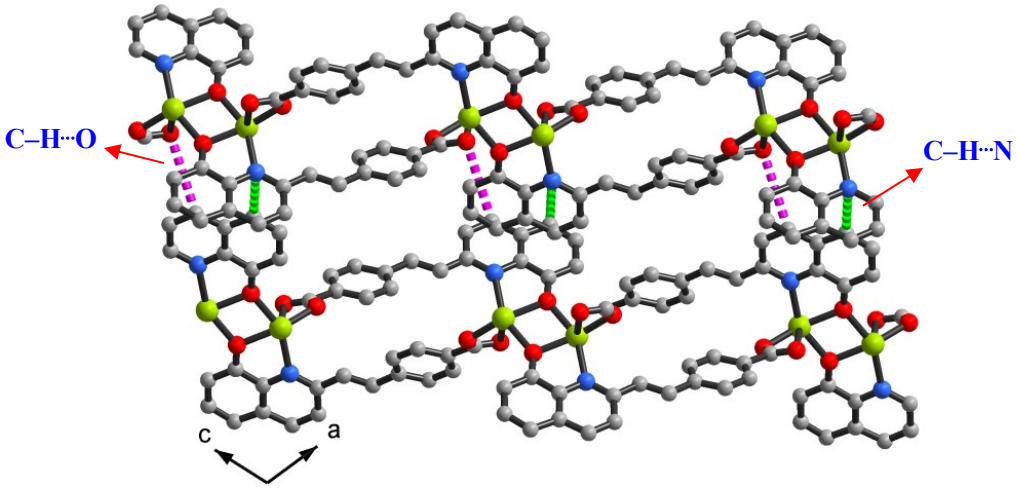

Figure S6. The *meso*-helical chains (*P* + *M*) in **1** along the *c* axis.

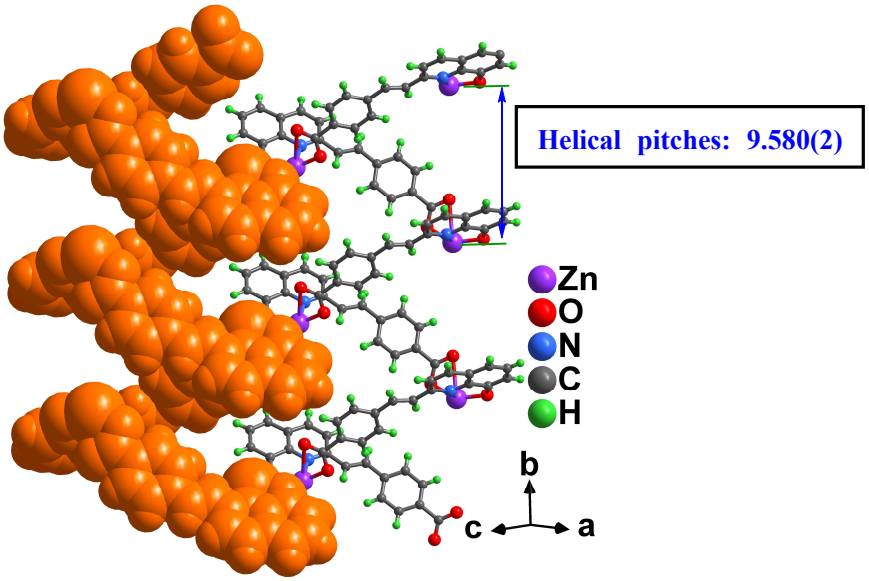

Figure S7. (a) View of the 3D structure in **1** (the space-filling mode of CH_3OH and coordinated DMF molecules protruding into the channels); (b) The space-filling mode of 3D network of **1**

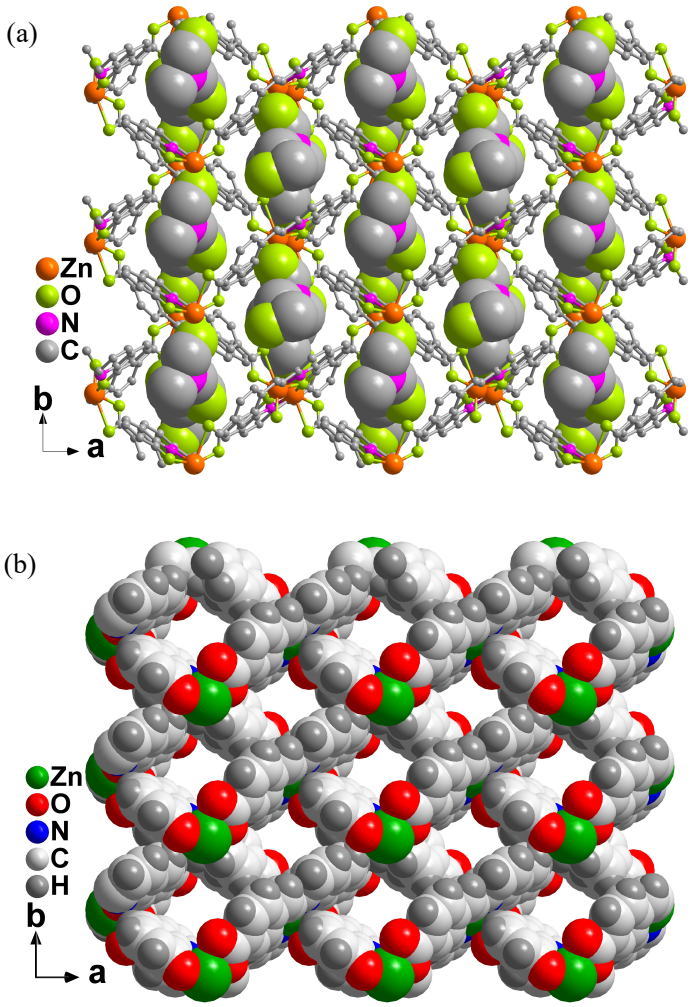

Figure S8. View of the asymmetric unit of **2**.

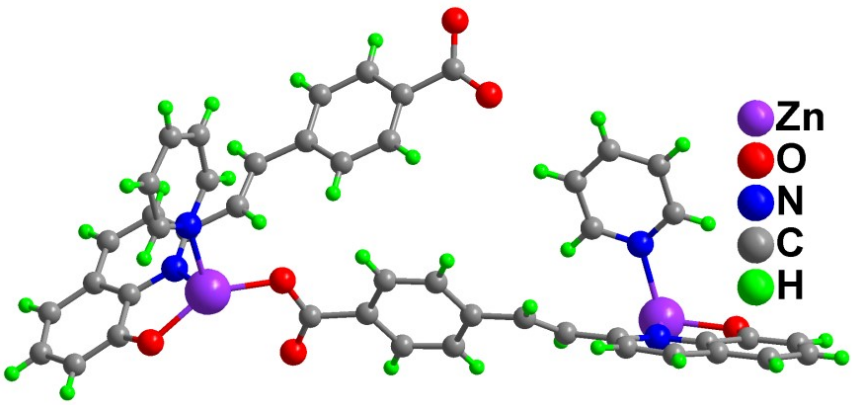

Figure S9. View of π···π stacking intramolecular interactions in **2.**

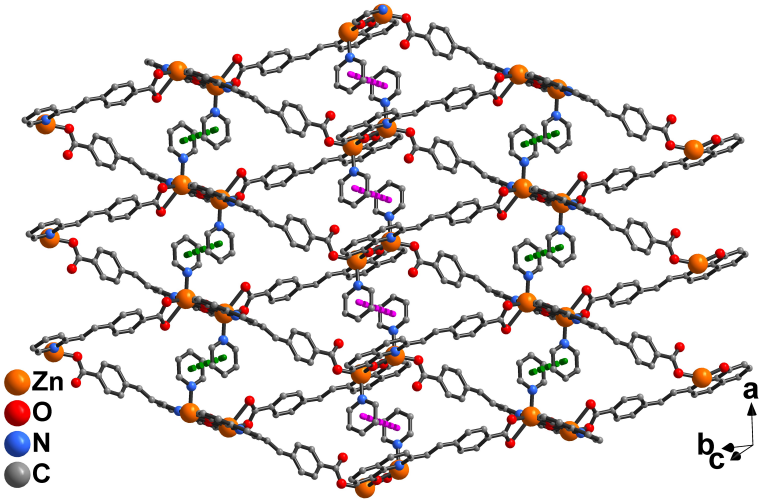

Figure S10. View of 3D stacking structure of **2.**

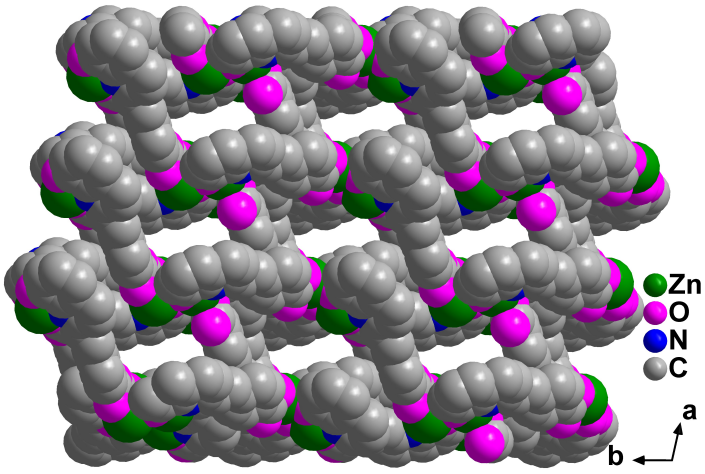

Figure S11. Perspective view of intermolecular π···π and C–H···O interactions in **2.**

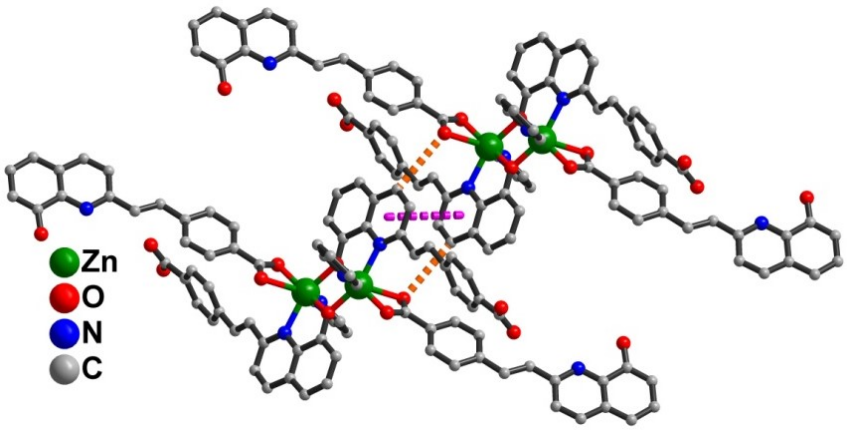

Figure S12. View of the asymmetric unit in **3**.

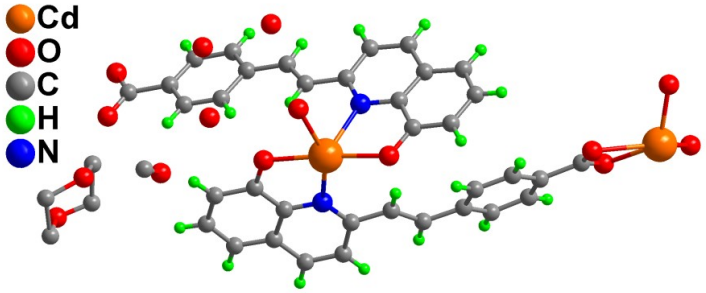

Figure S13. View of binuclear unit $[Cd_2(L)_4]$ in **3**.

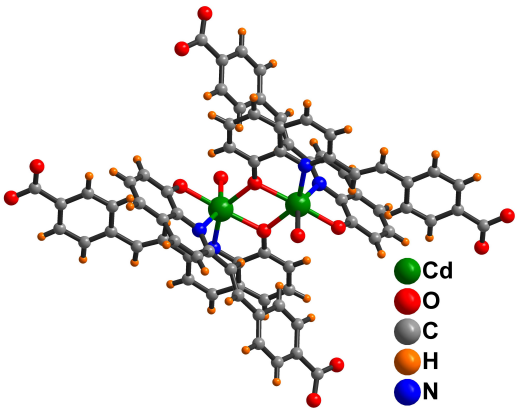

Figure S14. The 2D network structure of **3** in the *ab* plane.

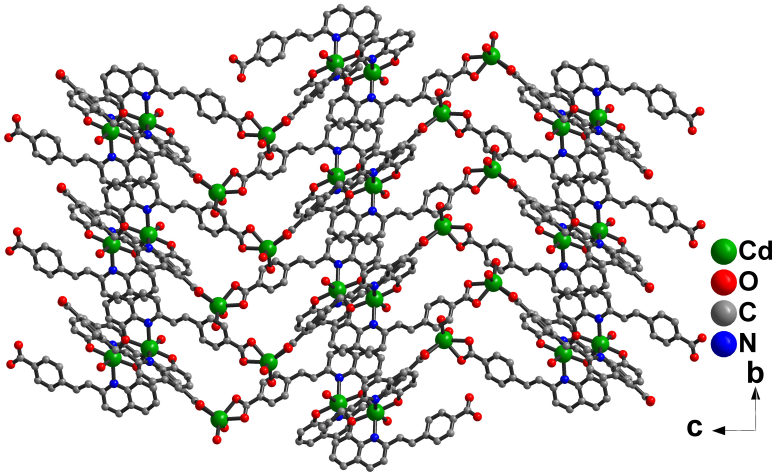

Figure S15. Perspective view of intramolecular π···π and C–H···π interactions in **3.**

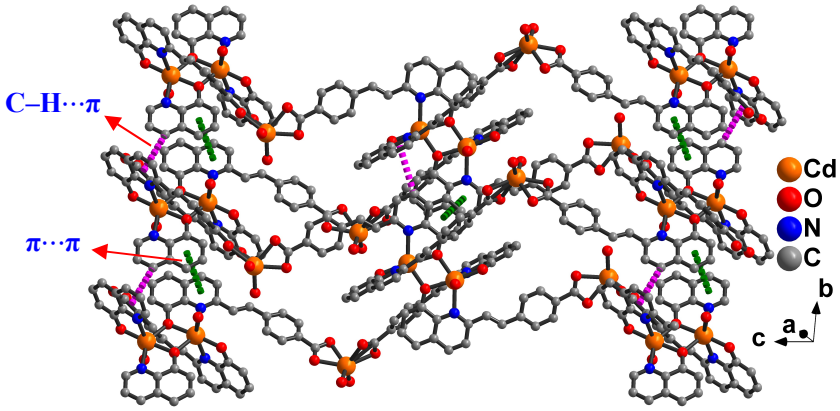

Figure S16. View of the asymmetric unit in **4.**

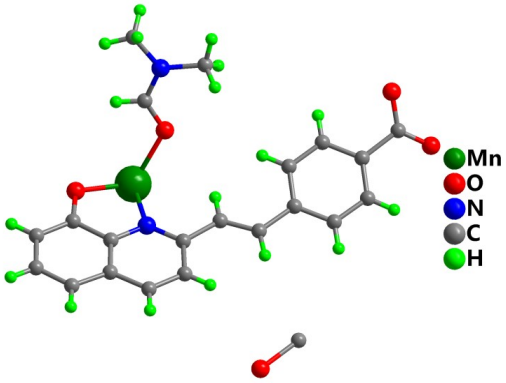

Figure S17. In **4**, each Mn is surrounded by two L to form a 2_1 helical chain running along the *b* axis.

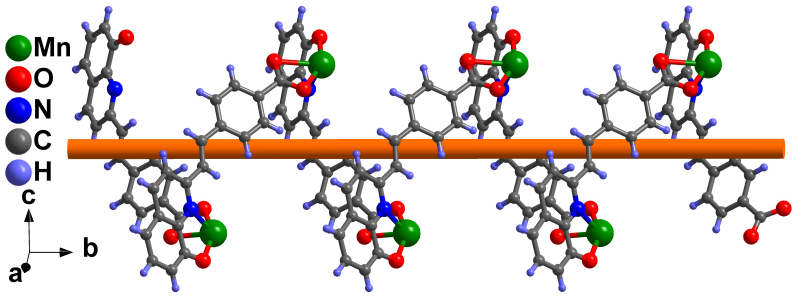

Figure S18. View of 3D supramolecular structure in **4** (The DMF molecules in channels are shown *via* the space-filling mode)**.**

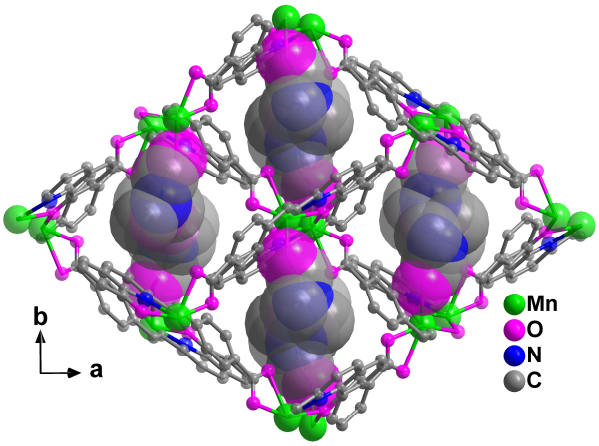

Figure S19. View of the asymmetric unit of complex **5**.

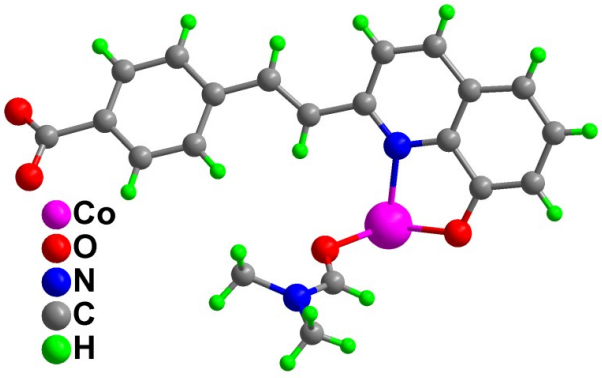

Figure S20. The coordination geometries of Co in **5**.

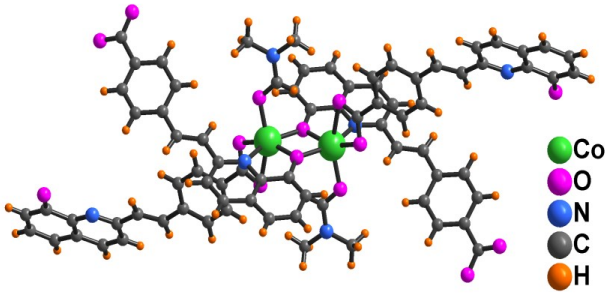

Figure S21. View of 2D structure of **5** built from binuclear units [Co_2L_4] (green polyhedron).

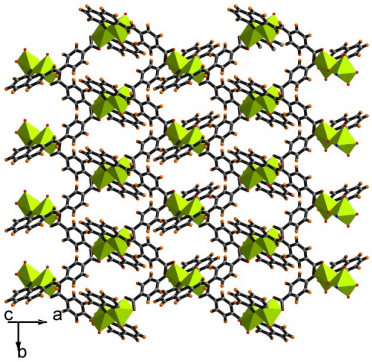

Figure S22. PXRD patterns of complexes **1**–**5**.

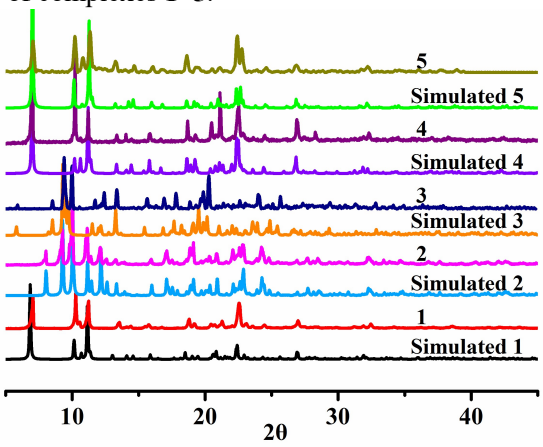

Figure S23. TGA plots for complexes **1**–**5**.

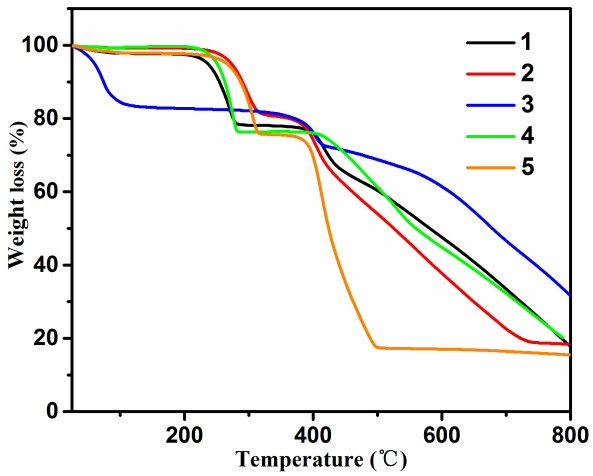

Figure S24. Fluorescence decay curves of free ligand H_2L and complexes **1**-**3** in the solid state.

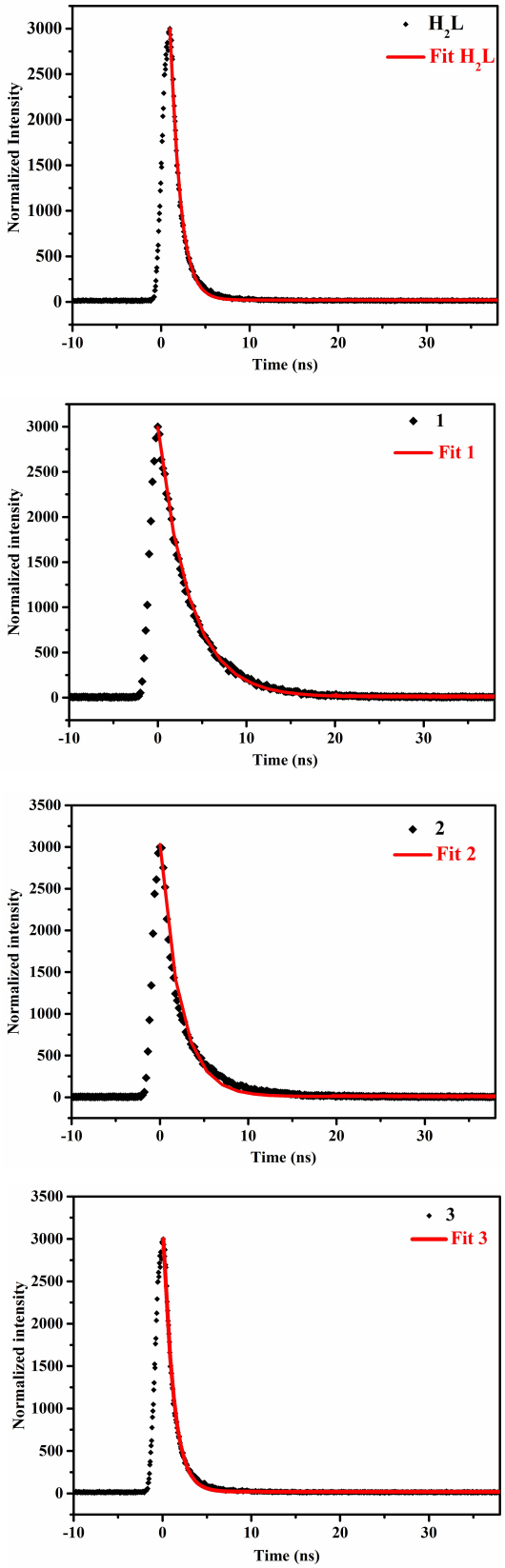

Figure S25. The fluorescence intensities of **1** in various organic molecules when excited at 350 nm.

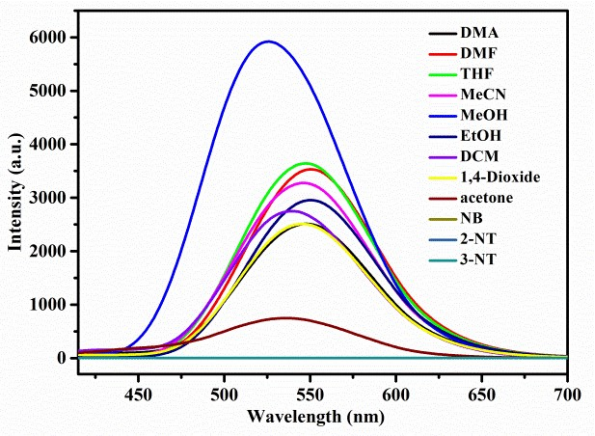

Figure S26. Fluorescence spectra of **1** upon addition of various amounts of nitrobenzene, *o*-nitrotoluene and *m*-nitrotoluene (NACs/MeOH=0.1 M), λ_{ex}= 350 nm.

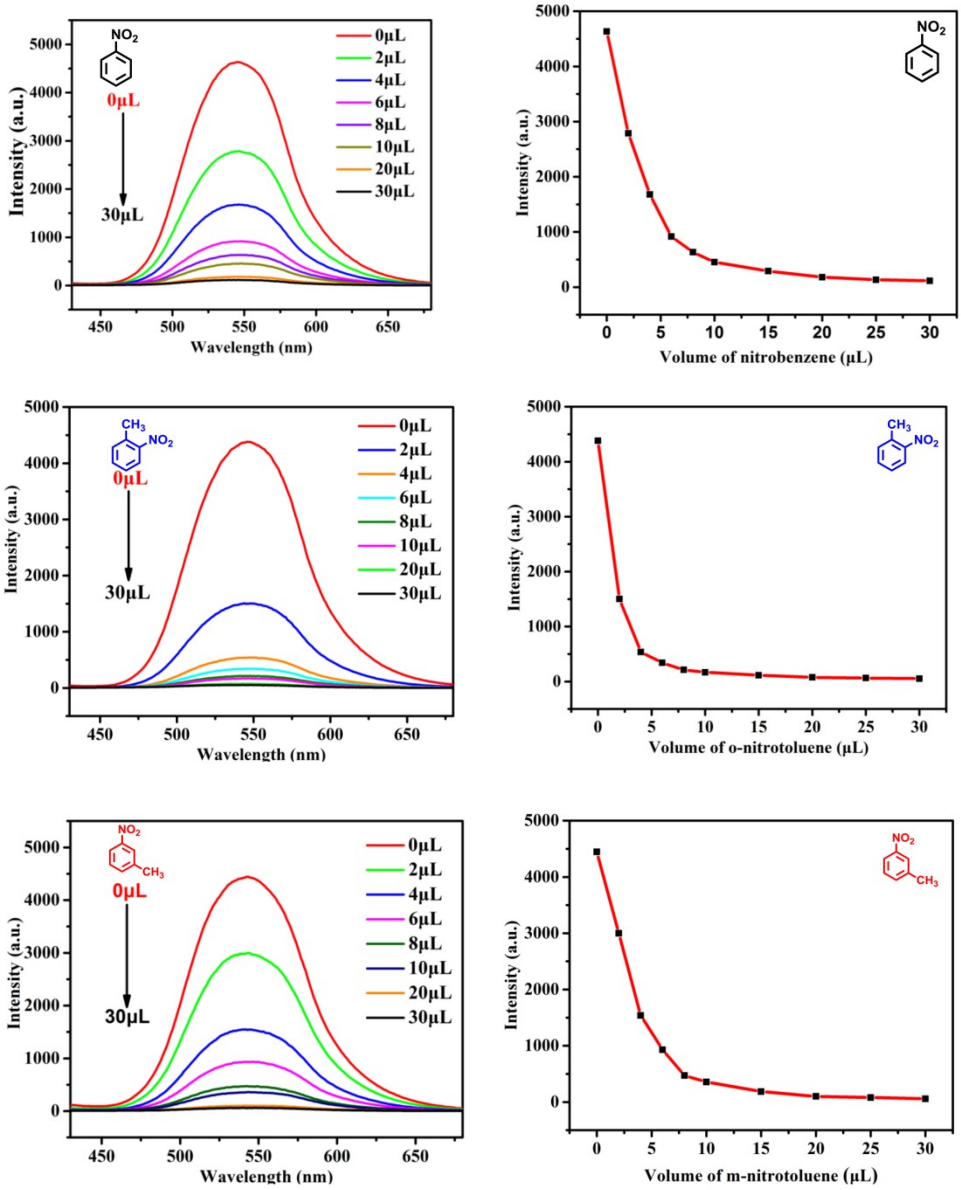

Figure S27. Luminescence spectra (a) and intensity (b) of **1** treated with various aromatic analytes (1.0×10^{-3} M in MeOH).

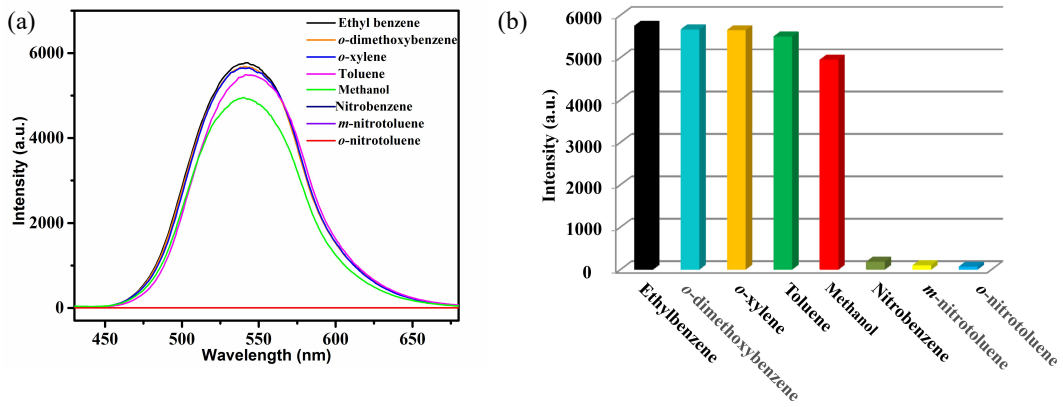

Figure S28. Upon addition of different Ln^{3+} cations, luminescence spectra (a) and intensity (b) of suspension of **1**.

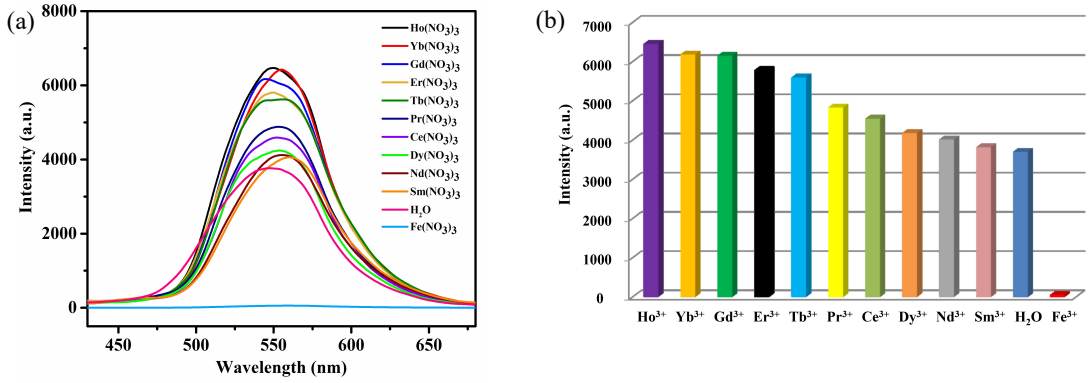

Figure S29. Luminescence intensities of **1** immersed in the individual aqueous solutions of $Ln(NO_3)_3$ (1 mM; red color) and mixed metal ions including Fe^{3+} ion (1 mM; blue color) under an excitation of 350 nm.

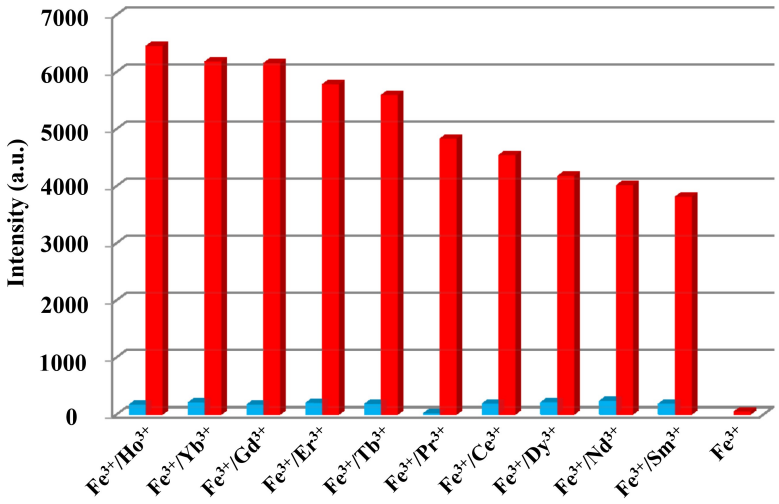

Figure S30. The reversibility test for sensing Fe^{3+}. Emission intensity of **1**, Fe@**1**, @**1**, 2nd, 5th.

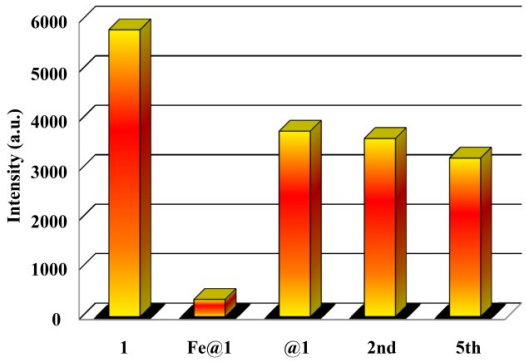

Emission intensity of **1**, Fe@**1**, @**1**, 2nd, 5th. (Noting: Fe@**1** sample dispersed in an iron nitrate solution sonicated for 30 minutes; @**1** is supersonic ultrasound, centrifuged and washed with distilled water until the solution is colorless; 2nd is the repeat experiment with the same batch of samples at second times; 5th is the fifth repeated test with the same sample.

Figure S31. PXRD patterns of **1** dispersed in water, **1** dispersed in an iron nitrate solution and the recycled sample.

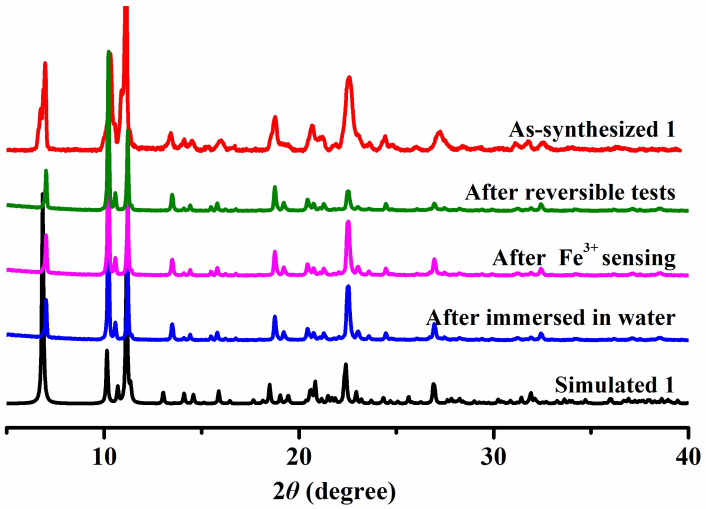

Figure S32. Variation of fluorescence intensities of complex **1** immersed in the aqueous solutions with different concentrations of $Fe(NO_3)_3$ (λ_{ex} = 350 nm).

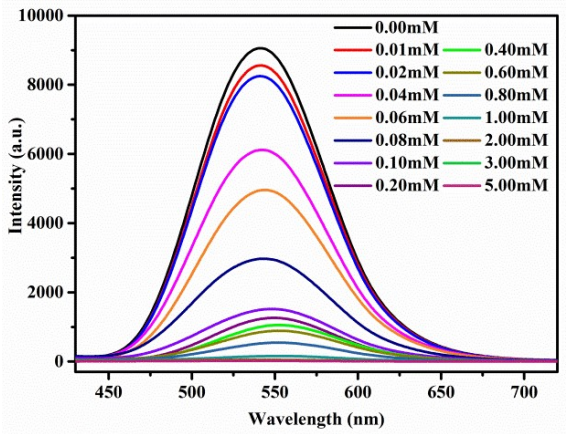

Figure S33. The fitting plot of the quenching efficiency with the increasing concentration of Fe^{3+} in the low concentration range, the red line corresponds to a fit to the linear relationship.

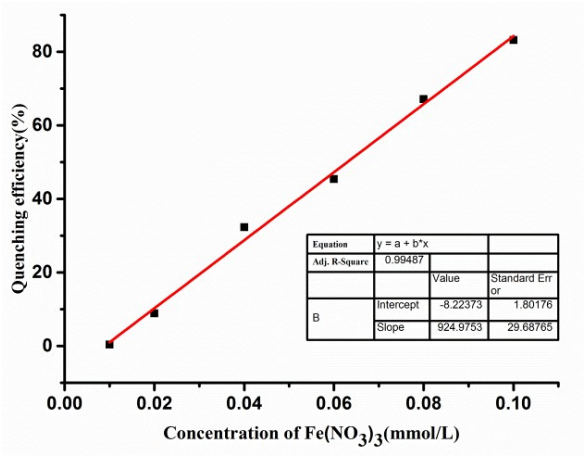

Figure S34. The UV−vis absorption spectra of aqueous solutions containing various mental ions ($M(NO_3)_x$ or $Ln(NO_3)_3$ or $FeSO_4$) with the same volume of 1×10^{-3} mol·L^{-1}, the excitation spectrum and the absorption spectra of **1** (2 mg) dispersed in water (2 mL).

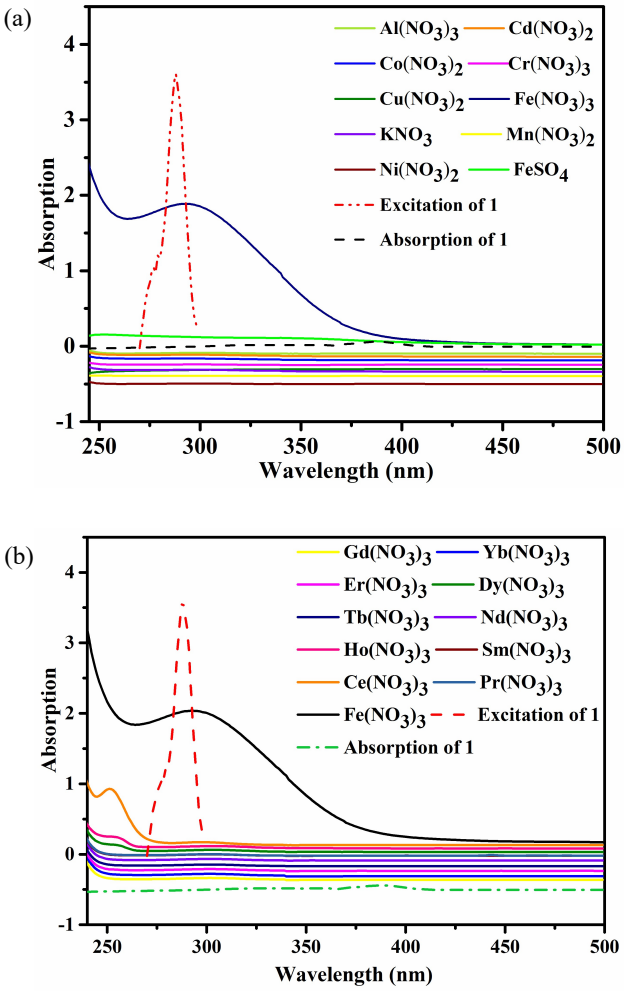
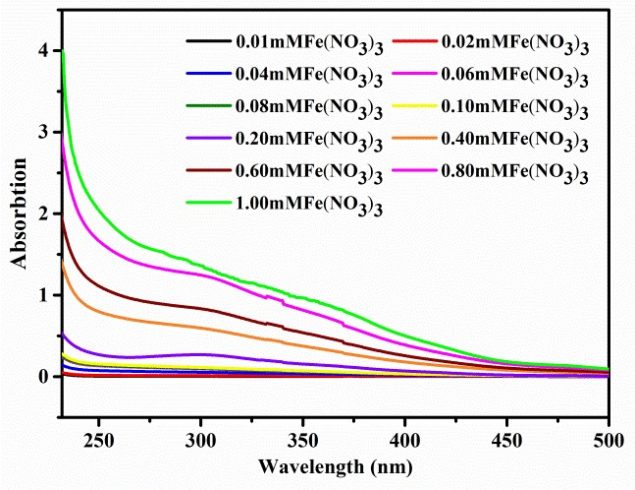
Figure S35. The UV−vis absorption spectra of Fe^{3+} with a gradual increase in concentration.